Proceedings of the Sixteenth International Conference on
Computational Structures Technology
Edited by: P. Iványi, J. Kruis and B.H.V. Topping
Civil-Comp Conferences, Volume 14, Paper 4.5
Civil-Comp Press, Edinburgh, United Kingdom, 2026
ISSN: 2753-3239, doi: 10.4203/ccc.14.4.5

Post-Fire Strength Capacity Assessment of SRC Columns Under Asymmetry Conditions

C.-G. Chiorean

Technical University of Cluj-Napoca, Structural Mechanics Department, Romania

Abstract

This study presents a unified computational framework for the direct assessment of the post-fire strength capacity of steel-reinforced concrete (SRC) cross-sections subjected to biaxial loading under geometric and thermal asymmetry. In contrast to conventional interaction-surface approaches, the proposed methodology reformulates strength assessment as a direct equilibrium–failure problem solved along prescribed loading paths, eliminating the need for interaction surface construction. The framework is built upon a hierarchical operator-based solution strategy comprising: (i) a predictor-based localization stage driven by a reduced sectional stiffness matrix, which identifies both the governing control pivot and a bracketing interval containing the failure point; (ii) an outer bisection procedure acting on a control strain parameter; and (iii) an inner damped Newton solver enforcing sectional equilibrium. To improve robustness under severe thermal degradation and material softening, an Adaptive Plastic Centroid (APC) formulation is introduced, providing a stable reference configuration and extending the solvability domain in regimes where classical formulations may become ill-conditioned. The framework consistently captures irreversible degradation and path-dependent thermo-mechanical effects throughout heating, cooling, and post-fire stages. Numerical results demonstrate excellent robustness and accuracy, while highlighting the critical influence of the cooling phase on the residual strength capacity of asymmetrically heated SRC cross-sections.

Keywords: strength capacity of cross-sections, bi-axial bending, fire analysis, composite steel-concrete, full-range fire, strain-driven

1 Introduction

Ultimate limit state analysis remains the cornerstone of structural design and safety assessment for reinforced concrete and composite steel–concrete systems subjected to combined axial force and biaxial bending. Accurate prediction of load-carrying capacity requires solving a highly nonlinear sectional equilibrium problem governed by complex constitutive behaviour, geometric nonlinearity, and strain compatibility conditions. In conventional practice, sectional resistance is typically evaluated through the construction of interaction surfaces or failure envelopes. Although rigorous, this approach becomes computationally expensive for composite cross-sections of arbitrary geometry and spatially varying material properties. Moreover, it requires an exhaustive exploration of the loading domain and does not directly provide the ultimate response associated with a prescribed load path. To overcome these limitations, direct strength assessment methods have been proposed for ambient temperature conditions, enabling the evaluation of ultimate capacity without constructing the full interaction surface [1, 2]. However, the extension of such approaches to fire conditions remains limited. Fire exposure introduces additional complexity due to strong temperature dependence of material properties, irreversible degradation mechanisms, and path-dependent thermo-mechanical effects. In most existing models, analysis is restricted to the heating phase and peak temperature state, while cooling and post-fire stages are often neglected. This simplification may lead to incomplete safety assessments, particularly in situations where structural stability during cooling or after fire extinction governs the actual failure scenario. Experimental and numerical evidence shows that significant stress redistribution, stiffness recovery effects, and delayed cracking may occur during the cooling phase due to thermal gradients and restrained contraction. Therefore, a consistent full-range fire formulation covering heating, cooling, and residual states is essential for realistic structural evaluation.

In this context, the present study proposes a unified APC-based direct nonlinear framework for SRC cross-sections subjected to biaxial loading throughout the complete fire history. The methodology reformulates strength assessment as a direct equilibrium-failure problem and combines a strain-driven sectional formulation with a hierarchical solution strategy comprising a predictor-based localization stage, an outer bisection procedure, and an inner damped Newton equilibrium solver. A key feature of the approach is the introduction of an Adaptive Plastic Centroid (APC) transformation, which improves numerical conditioning and solution robustness under severe geometric and thermal asymmetry. The main contributions of this work are: (i) the development of a direct nonlinear equilibrium framework for post-fire strength assessment without constructing interaction surfaces, (ii) the introduction of a predictor-based localization operator for identifying the governing control pivot and the admissible failure domain, (iii) the formulation of a robust nested Bisection–Newton strategy for reliable convergence under severe nonlinearities and material softening, (iv) the introduction of the Adaptive Plastic Centroid (APC) to improve solution uniqueness and numerical stability, and (v) the consistent treatment of heating, cooling, and post-fire residual states within a unified thermo-mechanical formulation.

2 Non-Linear Thermal Analysis and Phasic Material Properties

The temperature distribution $T(y,z,t)$ across the cross-section is determined transiently by solving the 2D nonlinear heat conduction equation using the finite element method (FEM):

$$\lambda\nabla^2 T = \rho c\frac{\partial T}{\partial t} \quad (1)$$

where λ is the thermal conductivity, c is the specific heat, and ρ is the material density. Heat exchange on the exposed boundaries is modelled through convection and radiation processes driven by the standard ISO 8364 fire curve, which incorporates a mandatory heating-cooling progression defined by EN 1991-1-2 [3]:

$$T_\infty = \begin{cases} 20 + 345\, log_{10}(8t+1)\,, heating\ phase\ (t \le t_h) \\ T_h - 10.417(t-t_h), t_h \le 30\ (t > t_h) \\ T_h - 4.167\left(3 - \frac{t_h}{60}\right)(t-t_h), 30 < t_h < 120\ (t > t_h) \\ T_h - 4.167(t-t_h), t_h \ge 120\ (t > t_h) \end{cases} \quad (2)$$

where T_∞ is the gas temperature (^{0}C) and t is the time of exposure to fire in minutes, T_h is the maximum temperature achieved in the heating stage (^{0}C), t_h is the duration of the heating stage in minutes [4].

To capture physical consistency during temperature abatement (i.e. $dT/dt \le 0$), the thermo-physical properties are treated differentially across the fire phases based on microstructural damage mechanics. Following advanced thermal calibration, the thermal conductivity during cooling is considered completely irreversible and locked at the minimum value corresponding to the local peak historical temperature ($T_{\max}$):

$$\lambda_{c,cooling}(T, T_{max}) = \lambda_c(T_{max}), \text{ for } \frac{dT}{dt} \le 0 \quad (3)$$

During heating, the specific heat features a massive peak between 100°C and 200°C due to the endothermic latent heat consumption of water vaporization. Once this vapour escapes, the process is finalized; water cannot condense back into the dehydrated pores during cooling. Thus, the specific heat during cooling does not retrace the moisture evaporation peak. It models a smooth, decreasing dry aggregate-matrix baseline:

$$c_{c,cooling}(T, T_{max}) = c_{dry}(T) \le c_c(T_{max}), \text{ for } \frac{dT}{dt} \le 0 \quad (4)$$

where $c_{dry}(T)$ represents the specific heat for dry concrete extracted from dry-concrete curves of EN 1992-1-2 as a function of the current lowered temperature T [3]. The concrete density during the cooling phase is limited by the minimum value attained at the maximum temperature $T_{\max}$, while subsequent evolution is governed solely by reversible thermal volumetric effects. Under this assumption, the density during cooling is expressed as:

$$\rho_{c,cooling}(T, T_{max}) = \rho_c(T_{max})[1 - 3\alpha_c(T_{max} - T)], \text{ for } \frac{dT}{dt} \le 0 \quad (5)$$

where $\rho_c(T_{max})$ denotes the concrete density at the maximum temperature reached during heating, inherently incorporating irreversible thermally induced mass losses, and α_c is the coefficient of thermal expansion of concrete. The term $3\alpha_c(T_{max} - T)$

represents the isotropic volumetric thermal contraction during cooling, consistent with EC2-type thermo-mechanical assumptions, while neglecting any recovery of chemically induced density changes.

The thermo-physical properties of structural steel and reinforcing steel, namely thermal conductivity λ_s, specific heat capacity c_s and density ρ_s are assumed to be fully reversible with respect to temperature. Accordingly, during the cooling phase, these properties are assumed to retrace their corresponding heating curves in the reverse order, with no hysteresis effects of irreversible thermal degradation considered.

2.1. Section Geometry and Kinematic Assumptions

Consider the cross-section subjected to the action of the external bending moment $\vec{\mathbf{M}}_O = M_z\vec{\mathbf{i}} + M_y\vec{\mathbf{j}}$ with scalar components (M_z, M_y) applied about global axes Oz (with unit vector $\vec{\mathbf{i}}$) and Oy (with unit vector $\vec{\mathbf{j}}$) respectively, and axial force $\vec{\mathbf{N}} = N\vec{\mathbf{k}}$ with scalar component (N) applied along the Ox axis (with unit vector $\vec{\mathbf{k}}$) as shown in Figure 1a [4]. Usually, the origin O is selected as either geometrical or plastic centroid of the cross-section.

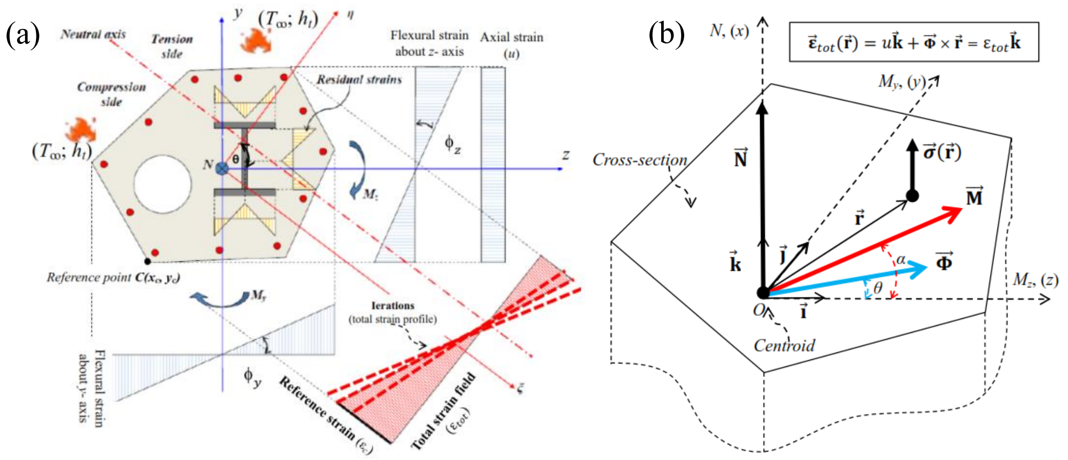

Figure 1: (a) Model of composite cross-section; (b) Positive sign convention.

The cross-section can have any shape with polygonal or circular openings, but the approach discussed in this paper is limited to composite steel-concrete sections where structural steel is partially or fully enclosed in concrete. Assuming plane sections remain plane after deformation, the strain distribution corresponding to curvatures $\vec{\boldsymbol{\Phi}}=[\phi_z \quad \phi_y]^T = \phi_z\vec{\mathbf{i}} + \phi_y\vec{\mathbf{j}}$ and axial strain u are expressed linearly at any point $\vec{\mathbf{r}} = [z \quad y]^T = z\vec{\mathbf{i}} + y\vec{\mathbf{j}}$ in the concrete matrix, structural steel, or reinforcement bars (Figure 1b) [4]. In line with Bernoulli plane section hypothesis, it is assumed that the total strain field varies linearly throughout the cross-section (Figure 1b):

$$\vec{\boldsymbol{\varepsilon}}_{tot}(\vec{\mathbf{r}}) = u\vec{\mathbf{k}} + \vec{\boldsymbol{\Phi}} \times \vec{\mathbf{r}} = \varepsilon_{tot}\vec{\mathbf{k}} \tag{6}$$

where × denotes the vector product. As a result, the total strain is assumed to follow an additive decomposition of mechanical and thermal strain as:

$$\varepsilon_{tot}\left(u,\phi_{z,}\phi_{y};T\right) = u + \phi_{z}y - \phi_{y}z = \varepsilon_{mech} + \varepsilon_{th}(T) \tag{7}$$

where ε_{mech} represents the mechanical strain and ε_{th} represents the thermal strain a function of the temperature T at the specified fiber. From Equation (2) the mechanical strain can be expressed:

$$\varepsilon_{mech}\left(u,\phi_{z},\phi_{y};T\right) = \varepsilon_{tot} - \varepsilon_{th} \tag{8}$$

and the implicit nonlinear constitutive material model for concrete and steel at high temperatures can be defined in the form:

$$\vec{\boldsymbol{\sigma}}(\vec{\mathbf{r}}) = \sigma\vec{\mathbf{k}}\ ;\ \sigma = \sigma(\varepsilon_{mech}) \tag{9}$$

The effect of concrete spalling at high temperatures is not considered in this formulation. The thermal analysis assumes reinforcement bar temperatures match the surrounding concrete, with perfect thermal contact between structural steel and concrete.

2.2. Thermo-Mechanical Constitutive Framework for Heating and Cooling Phases

A key limitation of conventional implicit constitutive models is their inability to distinguish between heat-then-load (HTL) and load-then-heat (LTH) paths, since transient strain effects are embedded implicitly within the formulation. In Eurocode 2 [3] the parabolic stress–strain relationship is calibrated primarily against HTL experimental data, leading to an apparent increase in peak strain $\varepsilon_{c1,T}^{EC2}$(often exceeding 0.01) to implicitly account for load-induced thermal strain (LITS). However, this approach becomes inconsistent during cooling, where LITS development ceases and the accumulated transient strain remains frozen, resulting in an LTH-type response [5].

$$\sigma_c(\varepsilon_{mech}) = \begin{cases} \dfrac{3\varepsilon_{mech}f_{c,T}}{\varepsilon_{c1,T}^{EC2}\left(2+\left(\frac{\varepsilon_{mech}}{\varepsilon_{c1,T}^{EC2}}\right)^{3}\right)}, heating\ \left(\frac{dT}{dt} > 0\right) \\ \dfrac{3\varepsilon_{mech}f_{c,T_{max}}}{\varepsilon_{c1,T_{max}}^{ENV}\left(2+\left(\frac{\varepsilon_{mech}}{\varepsilon_{c1,T_{max}}^{ENV}}\right)^{3}\right)}, cooling\ and\ post-fire\ \left(\frac{dT}{dt} \leq 0\right) \end{cases} \tag{10}$$

To overcome these limitations without introducing path-dependent internal variables, the physically-based model proposed by Le, Torero, and Dao (2021) is adopted [6]. The formulation retains the classical decomposition of strain as presented in Equation (8) while distinguishing the constitutive parameters depending on the thermal phase. The constitutive relationship is defined in Equation (10). Within this framework, concrete strength degradation is assumed irreversible, being governed solely by the maximum experienced temperature $T_{\max}$. The residual compressive strength is thus expressed as:

$$f_{c,cooling} = f_{c,T_{max}} = k_c(T_{max})f_{c0} \tag{11}$$

The peak strain parameter follows a phase-dependent definition. During heating, $\varepsilon_{c1,T}^{EC2}$ is adopted according to Eurocode 2, whereas during cooling it is replaced by the steady-state ENV formulation, evaluated at T_{max}:

$$\varepsilon_{c1,T_{max}}^{ENV} = \varepsilon_{c1,0}\left[1 + 1.5\left(\frac{T_{max}-20}{1000}\right) + 4.5\left(\frac{T_{max}-20}{1000}\right)^2\right] \tag{12}$$

This distinction prevents numerical inconsistencies such as strain overshooting or artificial stiffness locking during the cooling phase. Steel and reinforcing bars are assumed to follow a reversible thermal path [7, 8]. During cooling, their yield strength is recovered through interpolation between the degraded high-temperature state at T_{max} and the ambient condition at temperature T. Full recovery of mechanical properties, with no residual thermal strains, is assumed upon return to ambient temperature (T=20°C), such that:

$$f_{y,residual} = f_{y,0};\ E_{s,residual} = E_{s0} \tag{13}$$

To capture the thermo-mechanical response of concrete within a strain-driven sectional framework without resorting to computationally expensive history-dependent plasticity formulations, the free thermal strain ε_{th} is decomposed into three distinct thermodynamically consistent branches, following the reversal concept [8]:

$$\varepsilon_{th}(T, T_{max}) = \begin{cases} \varepsilon_{th,heating}(T), & heating\left(\frac{dT}{dt} > 0\right) \\ \varepsilon_{th,heating}(T_{max}) - \alpha_c(T_{max} - T), & cooling\left(\frac{dT}{dt} \leq 0, T > 20^oC\right) \\ \varepsilon_{res}(T_{max}), & post - fire(T = 20^oC) \end{cases} \tag{14}$$

The heating branch is governed by Eurocode 2 empirical expressions in functions of the type of aggregates; during cooling, thermal contraction is controlled by the effective coefficient α_c, defined as:

$$\alpha_c = \frac{\varepsilon_{th,heating}(T_{max}) - \varepsilon_{res}(T_{max})}{T_{max} - 20} \tag{15}$$

Finally, the post-fire residual strain $\varepsilon_{res}(T_{max})$ accounts for permanent shrinkage effects observed after complete cooling, as proposed by Gernay [8]:

$$\varepsilon_{res}(T_{max}) = \begin{cases} 0.0001\left(\frac{T_{max}-20}{100}\right), T_{max} \leq 400^oC \\ 0.0004 + 0.0005\left(\frac{T_{max}-400}{200}\right), 400^oC < T_{max} \leq 600^oC \\ 0.0009 + 0.0012\left(\frac{T_{max}-600}{400}\right), T_{max} \geq 600^oC \end{cases} \tag{16}$$

This permanent shrinkage induces significant kinematic incompatibilities within composite cross-sections. The outer layers, which cool faster, tend to contract earlier, while the core remains thermally expanded for a longer duration. This gradient generates tensile stresses in the outer concrete zones, promotes cracking, and leads to a redistribution of stiffness and a shift of the effective centroid of rigidity.

3 Formulation of the Proposed Mechanical Method

The analysis process involves two primary steps: (i) thermal analysis, which evaluates the temperature distribution across the cross-section at a given time, and

(ii) mechanical analysis, where the direct strength capacity is determined. A distinctive feature of the methodology developed here consists in direct assessment of the strength capacity of composite steel-concrete cross sections subjected to a specified load combination. The section, reported at the geometric or original plastic centroid (O), is assumed to be subjected to axial force N ($\vec{\mathbf{N}} = N\vec{\mathbf{k}}$) and bi-axial bending moment with components (M_z, M_y), $\vec{\mathbf{M}}_O = M_z\vec{\mathbf{i}} + M_y\vec{\mathbf{j}}$. The strength capacity can be characterized in two ways: either as ultimate strength capacity or nominal strength capacity. Each failure criterion establishes a specific state of strains and stresses, where further deformation leads to either a diminished response or breaches the predetermined conventional ultimate strain values [4]. The equilibrium is satisfied when the external forces $\vec{\mathbf{N}}$ (N) and $\vec{\mathbf{M}}_O$ (M_z, M_y) are equal to the internal ones and the corresponding failure criterion is fulfilled. These conditions can be explicitly represented in terms of the following nonlinear system of equations as:

$$\begin{cases} \vec{\mathbf{N}}_{int}\left(u, \phi_z, \phi_y\right) \equiv \int_\Omega \vec{\boldsymbol{\sigma}}(\vec{\mathbf{r}})d\Omega + \sum_b^{N_b} \vec{\boldsymbol{\sigma}}(\vec{\mathbf{r}}_b) \rightarrow N_{int}\vec{\mathbf{k}} - N = 0 \\ \vec{\mathbf{M}}_{int}\left(u, \phi_z, \phi_y\right) \equiv \int_\Omega \vec{\mathbf{r}} \times \vec{\boldsymbol{\sigma}}(\vec{\mathbf{r}})d\Omega + \sum_b^{N_b} \vec{\mathbf{r}}_b \times \vec{\boldsymbol{\sigma}}(\vec{\mathbf{r}}_b) \rightarrow M_{z_{int}}\vec{\mathbf{i}} + M_{y_{int}}\vec{\mathbf{j}} = \vec{\mathbf{M}}_O \\ + \\ \mathcal{F}\left(u, \phi_z, \phi_y\right) = 0 \end{cases} \tag{17}$$

where $\mathscr{F}(\bullet)$ represents the failure criterion [4], the surface integral is extended over steel and concrete areas (Ω) and Σ extends for all reinforcement bars, $A_{r,b}$ (b=1,N_b). The unknowns in the above nonlinear system of equations are the strain field parameters (u, ϕ_z, ϕ_y) together with the external load components (N, M_z, M_y). To determine a point on the interaction (failure) surface corresponding to a prescribed axial load and bending moment ratio, two additional linear constraints are imposed: (1) $N - N_O = 0$ and (2) $M_y - \tan(\alpha)M_z = 0$. Consequently, the strength capacity assessment problem is reduced to solving the following system of three coupled nonlinear equations:

$$\begin{cases} N_{int}\left(u, \phi_z, \phi_y\right) - N_O = 0 \\ M_{y_{int}}\left(u, \phi_z, \phi_y\right) - \tan(\alpha)\, M_{z_{int}}\left(u, \phi_z, \phi_y\right) = 0 \\ \mathcal{F}\left(u, \phi_z, \phi_y\right) = 0 \end{cases} \tag{18}$$

which defines a single point on the failure surface shown schematically in Figure 2a.

The proposed solution procedure consists of two consecutive stages. In the first stage, *a predictor-based bracketing strategy* is employed to identify an interval of the control strain, [ε_c^a; ε_c^b], containing the failure point. In the second stage, the failure condition is enforced through *a nested bisection-Newton procedure*, in which the outer bisection loop updates the control strain while the inner Newton solver satisfies sectional equilibrium for each trial value.

3.1. Predictor-Based Bracketing Phase

Considering the irregular composite section shown in Figure 1a, the orientation of the incremental neutral axis (i.e., the locus of zero incremental strain) is obtained from the incremental curvatures $\Delta\phi_z$ and $\Delta\phi_y$, predicted using the reduced stiffness matrix $\mathbf{K}_M = \mathbf{K}_{\phi\phi} - \mathbf{K}_{\phi u}\mathbf{K}_{uu}{}^{-1}\mathbf{K}_{u\phi}$ [4]. Based on this predicted strain field, the concrete vertex exhibiting the maximum incremental strain rate is identified and selected as a control pivot with coordinates (z_c, y_c). Once the critical node c is identified, a controlled incremental strain $\Delta\varepsilon_c$ is imposed. The corresponding target strain at this pivot for load step k is prescribed as:

$$\varepsilon_c^p = \varepsilon_c^{old} + \Delta\varepsilon_c \tag{19}$$

with

$$\varepsilon_c^{old} = u_{k-1} + \phi_{z,k-1}y_c - \phi_{y,k-1}z_c \tag{20}$$

The control pivot and its prescribed strain remain fixed throughout the equilibrium iterations associated with the current trial state. Assuming the prescribed strain value ε_c^p at the control point, the axial strain u can be expressed in terms of this reference strain. The total strain distribution associated with the curvatures $\phi_{z,k}$ and $\phi_{y,k}$ is then represented linearly with respect to these curvatures, leading to the additive decomposition:

$$u = \varepsilon_c^p - \left(\phi_{z,k}y_c - \phi_{y,k}z_c\right); \tag{21}$$

$$\tilde{\varepsilon}_{tot}\left(\phi_{z,k}, \phi_{y,k}\right) = \varepsilon_c^p + \phi_{z,k}(y - y_c) - \phi_{y,k}(z - z_c) \tag{22}$$

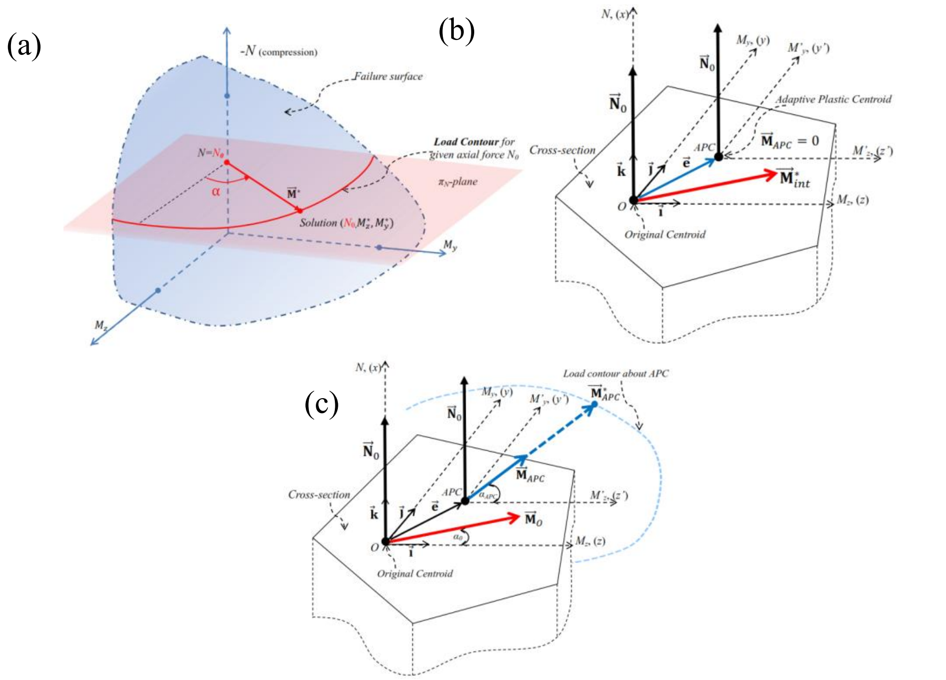

Figure 2: (a) Moment capacity contour; (b) Adaptive plastic centroid (APC); (c) Equivalent forces and load contour about APC.

The last equation of nonlinear system (18) can be decoupled from the first two equations. Treating curvatures $\phi_{z,k}$ and $\phi_{y,k}$ as independent variables of ε_c^p the first two equations can be solved, independently using the prescribed strain $\varepsilon_c = \varepsilon_c^p$. For each successive trial values of ε_c^p, the equilibrium problem, defined by the first two equations of the system (18), is solved using the Newton scheme enhanced by a damped strategy for stable convergence [4], yielding the curvature response $(\phi_{z,k}^*, \phi_{y,k}^*)$. This stage is continued only until a sign change of the failure function $\mathcal{F}(\phi_{z,k}^*, \phi_{y,k}^*; \varepsilon_c^p)$ is detected, thereby identifying a bracketing interval $[\varepsilon_c^a; \varepsilon_c^b]$, containing the failure point. The predictor-based localization stage may be represented symbolically through the operator $\mathcal{L}_{\mathbf{K}_M}$:

$$[\varepsilon_c^a; \varepsilon_c^b] = \mathcal{L}_{\mathbf{K}_M}\{\mathcal{F}[\mathcal{N}_{\mathbf{\Phi}^{0,*}}(\mathbf{F}(\mathbf{\Phi}, \varepsilon_c^p) = \mathbf{0}, \mathbf{\Phi}), \varepsilon_c^p]\} \tag{23}$$

where $\mathcal{L}_{\mathbf{K}_M}$ denotes *a predictor-based localization operator* driven by the incremental response direction obtained from the reduced stiffness matrix $\mathbf{K}_M$, $\mathbf{F}$ denotes the residual vector associated with the first two equations of the system (18). The damped-Newton sequences $\mathcal{N}_{\mathbf{\Phi}^0}$ is symbolically represented as:

$$\mathbf{\Phi}^* = \mathcal{N}_{\mathbf{\Phi}^{0,*}}\left(\mathbf{F}(\mathbf{\Phi}, \varepsilon_c^p) = \mathbf{0}, \mathbf{\Phi}\right) \tag{24}$$

in which $\mathbf{\Phi}^*$ is the solution obtained for a prescribed value of ε_c^p, starting with initial approximation $\mathbf{\Phi}^{0,*}$. The operator $\mathcal{L}_{\mathbf{K}_M}$ performs two coupled tasks. First, based on the incremental curvature direction predicted by $\mathbf{K}_M$, it identifies the control pivot *c*, defined as the concrete vertex exhibiting the maximum incremental strain rate. Second, successive trial values of the prescribed strain ε_c^p are generated at this pivot and the corresponding equilibrium states are computed through the Newton operator. The failure function $\mathcal{F}(\mathbf{\Phi}^*, \varepsilon_c^p)$ is subsequently evaluated and monitored for a sign change. The localization process terminates once

$$\mathcal{F}(\mathbf{\Phi}^*, \varepsilon_c^a)\mathcal{F}(\mathbf{\Phi}^*, \varepsilon_c^b) < 0 \tag{25}$$

which defines the bracketing interval $[\varepsilon_c^a; \varepsilon_c^b]$ containing the failure point. During the predictor-based localization stages, the control pivot *c* may be updated according to the evolution of the incremental strain field over successive trial states, and is finally retained as the last configuration associated with the sign change of the failure function. Once the bracketing interval has been established, the identified pivot *c* is fixed and used as the reference point for the control strain. The failure point is then obtained through a nested bisection-Newton procedure, where the outer bisection loop refines ε_c^p at the fixed pivot and the inner damped Newton solver enforces sectional equilibrium.

3.2. Nested Bisection-Newton Phase

After the bracketing interval has been identified, the failure point is determined by an outer bisection procedure acting on the prescribed strain ε_c^p. For each strain value generated by the bisection algorithm, the equilibrium equations are solved through the Newton procedure as described by Equation (24). The failure condition is then re-evaluated. This nested process continues until convergence is achieved both in equilibrium and in the failure criterion. At convergence, the solution set $(\phi_z = \phi_z^*; \phi_y = \phi_y^*)$ and the reference strain $\varepsilon_c^p = \varepsilon_c^*$ defines the strain and curvature state corresponding to the failure point on the interaction surface. The complete nested Bisection-Newton scheme can be summarized as:

$$\varepsilon_c^* = \mathcal{B}_{\varepsilon_c^a}^{\varepsilon_c^b}\{\mathcal{F}[\mathcal{N}_{\boldsymbol{\Phi}^{0,*}}(\mathbf{F}(\boldsymbol{\Phi},\varepsilon_c^p) = \mathbf{0},\boldsymbol{\Phi}),\varepsilon_c^p] = 0,\varepsilon_c^p\} \tag{26}$$

where $\mathcal{B}_{\varepsilon_c^a}^{\varepsilon_c^b}$ indicates *the Bisection operator* applied in the bracketing interval $[\varepsilon_c^a;\ \varepsilon_c^b]$ for failure equation $\mathcal{F}(\boldsymbol{\Phi}^*,\varepsilon_c^p) = 0$ with unknown ε_c^p and for known curvatures $\boldsymbol{\Phi}^*$ provided by the inner Newton solver as defined above and associated to different attempts for ε_c^p.

3.3. Details of the implementation

For a prescribed axial force N_0 and bending moment ratio tan(α)= M_y/M_z, unsymmetrical (geometric or thermal) cross-sections may exhibit non-uniqueness or loss solution existence when loading state lies outside the iso-load domain [4]. To ensure robustness, the formulation is transferred from the original centroid O to the *adaptive plastic centroid (APC)*, which provides a physically consistent reference configuration for highly nonlinear regimes. The APC position $\vec{\mathbf{e}} = e_z\vec{\mathbf{i}}+e_y\vec{\mathbf{j}}$ is defined such that the axial force N_0 produces a purely uniform stress state without bending:

$$\vec{\mathbf{M}}_{APC} \equiv \vec{\mathbf{M}}_{int}^* - \vec{\mathbf{e}} \times \vec{\mathbf{N}}_0 = \vec{0} \tag{27}$$

leading to the equivalent bending components:

$$M_{zAPC} = M_{zO} - N_0 e_y; M_{yAPC} = M_{yO} + N_0 e_z; \tag{28}$$

and a modified ratio $tan(\alpha_{APC}) \neq tan(\alpha_O)$. Since both representations ($\vec{\mathbf{N}}_0$, $\vec{\mathbf{M}}_O$) and ($\vec{\mathbf{N}}_0$, $\vec{\mathbf{M}}_{APC}$) are statically equivalent, the strain-stress field remain unchanged. Consequently, the strength analysis is performed with respect to the APC configuration, which significantly improves robustness and avoids ill-posed response paths.

The solution is initialized from a uniform strain state corresponding to N_0 with zero curvature ($\phi_z = \phi_y = 0$). The reduced stiffness matrix $\mathbf{K}_M$ is then evaluated under constant axial force [4], providing an estimation of the initial curvature direction:

$$\bar{\boldsymbol{\Phi}} = \mathbf{K}_M^{-1}\mathbf{f}, \qquad \mathbf{f} = [M_{yAPC} \quad M_{zAPC}]^T \tag{29}$$

A scaled initial state is constructed as:

$$\boldsymbol{\Phi}^{0,*} = \alpha\bar{\boldsymbol{\Phi}} \tag{30}$$

where the scalar α is chosen such that the prescribed reference strain $\varepsilon_c^p = \varepsilon_c^{p,0}$, typically taken as the minimum ultimate strain ($\varepsilon_{t,ult}^{min}$) from the ultimate strain surface [4], is satisfied at the control fibre. This provides a stable starting point for the nonlinear solution even in strongly unsymmetrical configurations.

Due to the strongly nonlinear response and pronounced material softening of composite cross-sections at elevated temperatures, a fixed prescribed strain increment $\Delta\varepsilon_c$ may lead to loss of convergence of the inner damped Newton corrector. In particular, large increments of the control strain may place the trial state outside the convergence basin of the Newton iteration, resulting in poor consistency between the updated curvature field and the assumed initial guess. If the damped-Newton scheme fails to converge within a prescribed maximum number of iterations (I_{max}), the current increment is rejected and the algorithm is rolled back to the last converged state k. To ensure robustness of the localization process under strongly nonlinear response and pronounced material softening, the strain increment is controlled through an adaptive operator $\mathcal{A}_{\Delta\varepsilon}$, embedded within the predictor-based loading path. The evolution of the prescribed strain increment is defined as:

$$\Delta\varepsilon_c^{k+1} = \mathcal{A}_{\Delta\varepsilon}\left(I_{conv}^{(k)}\right)\Delta\varepsilon_c^k \tag{31}$$

where $I_{conv}^{(k)}$ denotes the number of Newton iterations required for convergence at step k. The adaptive operator is defined as:

$$\mathcal{A}_{\Delta\varepsilon} = \begin{cases} \eta_d, I_{conv} > I_{max} \\ 1, I_{low} < I_{conv} \le I_{max} \\ \eta_i, I_{conv} \le I_{low} \end{cases} \tag{32}$$

with typical values $\eta_d = 1/2$, $\eta_i = 1.5$ and thresholds $I_{max} = 10$, $I_{low} = 4$.

4 Computational Examples

The composite steel–concrete cross-section shown in Figure 3a, comprising reinforced concrete, a structural steel profile, and a circular opening, was analyzed under the ISO 834 heating–cooling fire scenario. Material thermal and mechanical properties were adopted from Eurocode 2 and Eurocode 3 [4, 9, 10]. Owing to the lack of direct benchmark solutions for post-fire strength assessment, the proposed method was first validated against the elevated-temperature moment-capacity diagrams reported by Kim [10]. Figure 3b shows the capacity domains for an axial force of -4120 kN at different fire exposure times, demonstrating close agreement with the reference results.

The computational efficiency of the procedure is summarized in Table 1 and Figure 4 for a prescribed axial load of -6200 kN and various bending moment ratios. The method successfully handles challenging cases involving loads outside the iso-load contour and multiple solutions for the same loading direction. The analysis was subsequently extended to the complete fire history, including heating, cooling, and post-fire stages. For a heating duration of 2 h, the minimum strength capacity was reached during the cooling phase, approximately 3 h after fire ignition (Figure 5), highlighting the importance of considering the full fire cycle in residual strength assessments.

To further demonstrate the applicability of the proposed framework to geometrically and thermally asymmetric members, an L-shaped reinforced concrete column tested by Xu and Wu [11] was analyzed. The specimen was exposed to fire on three sides, resulting in a highly non-uniform temperature field and asymmetric stiffness degradation. Good agreement was obtained between predicted and measured temperatures at selected thermocouple locations (Figure 6a).

For an applied axial load of -2517 kN, the proposed model predicted failure after 188 min of fire exposure, compared with 207 min measured experimentally and 175 min reported by Xu and Wu [11]. The corresponding moment-capacity diagrams show a pronounced contraction and shift of the resistance domain with increasing fire exposure, reflecting the combined effects of thermal degradation and cross-sectional asymmetry (Figure 6b).

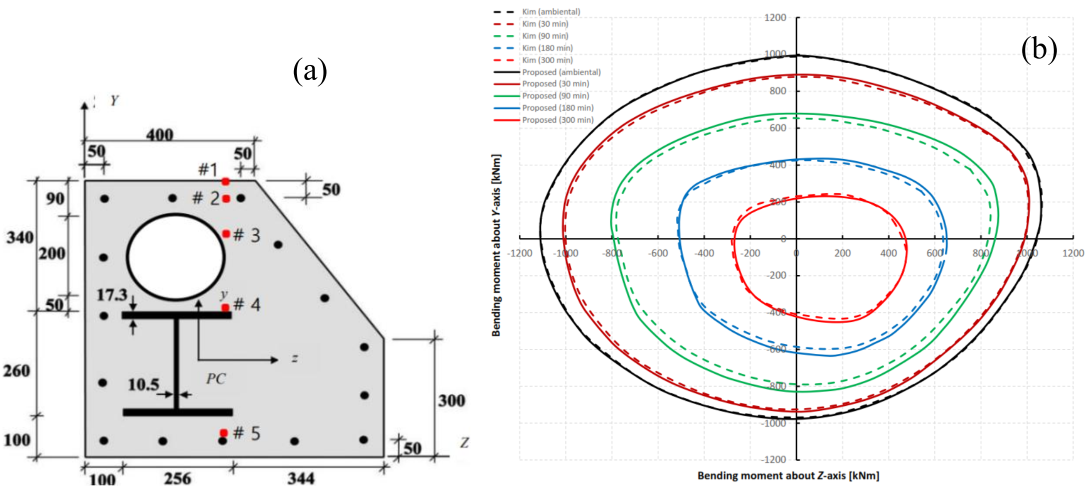

Figure 3: (a) Composite section; (b) Moment capacity contours (validation).

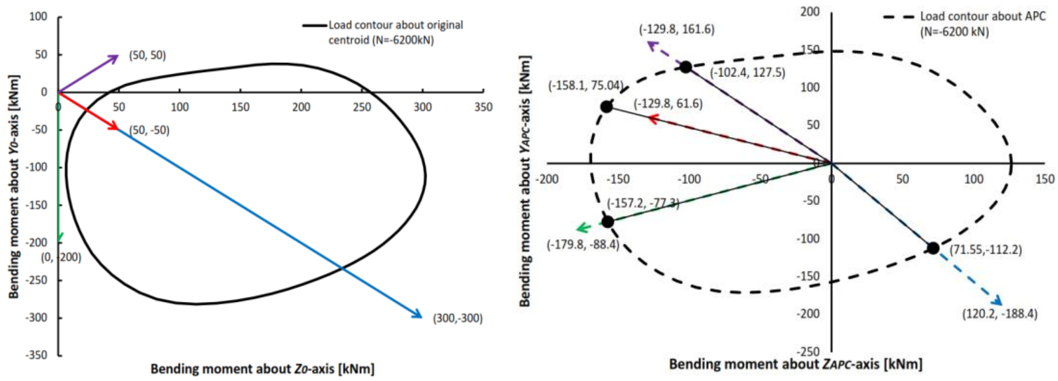

Figure 4: Loading scenarios about original and adaptive plastic centroid: N=-6200 kN.

Axial force N_0 [kN]	Moments about original centroid [kNm]		Moments about APC [kNm]		Moments capacity [kNm]		Check Strength Criteria
	M_{z0}	M_{y0}	M_{zAPC}	M_{yAPC}	M^*_{zAPC}	M^*_{yAPC}	$\lVert\vec{\mathbf{M}}_{APC}\rVert \leq \lVert\vec{\mathbf{M}}^*_{APC}\rVert$
-6200	50	-50	-129.8	61.6	-158.1	75.04	Yes
	300	-300	120.2	-188.4	71.55	-112.2	No
	50	50	-129.8	161.6	-102.4	127.5	No
	0	-200	-179.8	-88.4	-157.2	-77.3	No

Table 1: Direct strength assessment

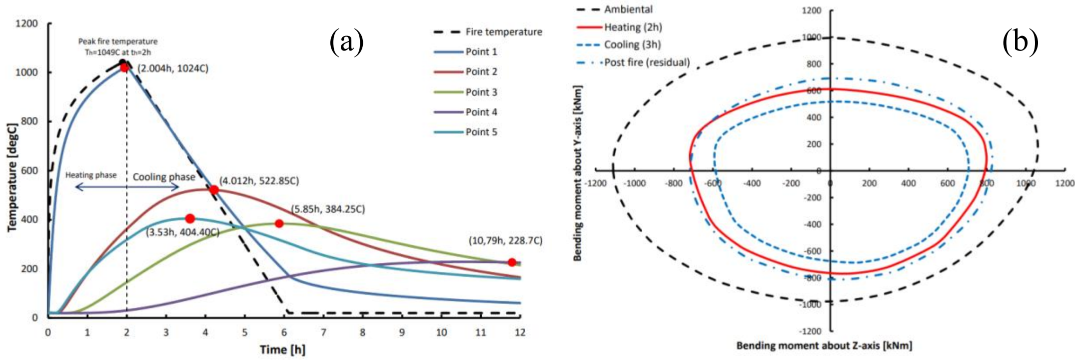

Figure 5: (a) Temperature-time curves and (b) Strength capacity (N=-4120kN) during heating, cooling and post fire phases.

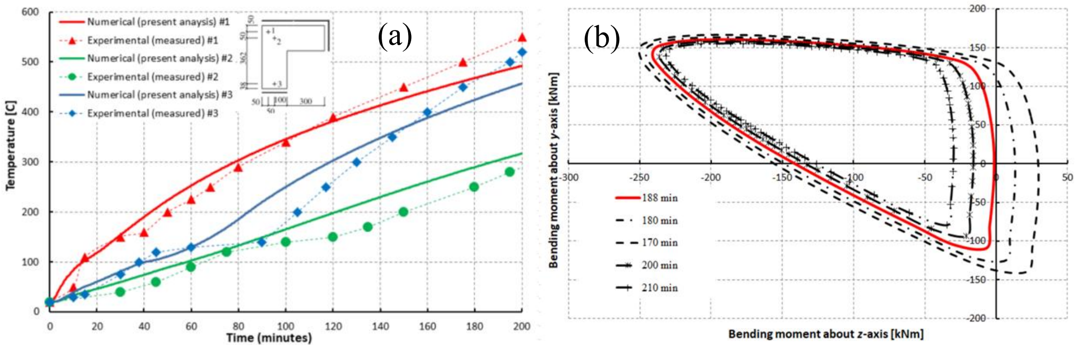

Figure 6: (a) Predicted temperatures and (b) Moment–capacity diagrams.

5 Conclusions and Contributions

This study presents a unified computational framework for the direct evaluation of the strength capacity of steel-reinforced concrete (SRC) cross-sections subjected to biaxial loading throughout the complete fire history, including heating, cooling, and post-fire stages. In contrast to classical interaction-surface construction strategies, the problem is reformulated as a direct nonlinear equilibrium-failure root-finding problem along prescribed load paths, eliminating the need for pre-computed strength domains. The main contributions are summarized as follows:

- A predictor-based localization operator is introduced to identify a bounded interval containing the failure point by exploiting the incremental response direction of the reduced stiffness matrix.
- A nested bisection-Newton strategy is developed, combining an outer bisection loop on the control strain with an inner damped Newton solver for sectional equilibrium, ensuring robust convergence under severe nonlinearities.
- The adaptive plastic centroid (APC) is employed as a consistent reference configuration, improving numerical conditioning and restoring solution stability in strongly unsymmetrical thermal states.
- Results show that minimum capacity may occur during cooling, highlighting the necessity of full fire-history analysis.

- The proposed formulation provides a computationally efficient reduced-order thermo-mechanical framework, capturing degradation and transient thermal effects without full path-dependent plastic integration.

Overall, the method establishes a robust and scalable operator-based framework for direct strength assessment of SRC cross-sections under extreme thermo-mechanical loading conditions.

References

[1] S.F. Chen, J.G. Teng, S.L. Chan, "Design of biaxially loaded short composite columns of arbitrary section" J Struct Eng, 127, 840-846, 2001.

[2] L. Rosati, F. Marmo, R. Serpieri, "Enhanced solution strategies for the ultimate strength analysis of composite steel-concrete sections subject to axial force and biaxial bending" Comp. Meth. App. Mech. Eng., 197, 1033-1055, 2008.

[3] CEN. EN 1991-1-2, Eurocode 1: Actions on structures, part 1.2: General actions-actions on structures exposed to fire. Brussels, Belgium: Comité Européen de Normalisation, 2002.

[4] C.G. Chiorean, "Computational issues in biaxial bending capacity assessment of RC and composite cross-sections exposed to fire". Comput. Struct., 302, 107477, 2004.

[5] G. Torelli, P. Mandal, M. Gillie, V.X. Tran, "Concrete strains under transient thermal conditions: A state-of-the-art review", Eng. Struct., 127, 172-188, 2016.

[6] Q.X. Le, J.L Torero, V.T. Dao, "Stress-strain-temperature relationship for concrete." Fire Safety J., 120, 103126, 2021.

[7] H. Yang, L.H. Han, Y.C. Wang, "Effects of heating and loading histories on post-fire cooling behaviour of concrete-filled steel tubular columns. J Constr Steel Res, 54, 556–70, 2008.

[8] T. Gernay, "Fire resistance and burnout resistance of reinforced concrete columns", Fire Safety J., 104, 67-78, 2019.

[9] C.G. Chiorean, "Direct strength capacity assessment of bi-axially loaded SRC cross-Sections exposed to full-range fire", In: Yang, J., Fu, J., Liu, A., Ng, CT. (eds), Proceedings of the First International Conference on Engineering Structures. ICES 2024. Lecture Notes in Civil Engineering, vol 599. Springer, Singapore, 2024.

[10] H.S. Kim, "Obtaining interaction diagram of concrete section exposed to fire by mathematical optimization". J Build Eng, 44, 102993., 2021.

[11] Y.Y. Xu, B. Wu, "Fire resistance of reinforced concrete columns with L-, T-, and +- shaped cross-sections", Fire Safety Journal, 44, 869-880, 2009.